BBA Advances 2 (2022) 100039

Contents lists available at ScienceDirect

BBA Advances

journal homepage: www.sciencedirect.com/journal/bba-advances

Cerosomes as skin repairing agent: Mode of action studies with a model stratum corneum layer at liquid/air and liquid/solid interfaces

Fabio Strati [a], Tetiana Mukhina [b], Reinhard H.H. Neubert [a], Lukas Opalka [c], Gerd Hause [d], Christian E.H. Schmelzer [a,e], Matthias Menzel [e], Gerald Brezesinski [a,*]

[a] Institute of Applied Dermatopharmacy at Martin Luther University Halle-Wittenberg, Weinbergweg 23, D-06120 Halle (Saale), Germany
[b] Institute for Condensed Matter Physics, TU Darmstadt, Hochschulstraße 8, 64289 Darmstadt, Germany
[c] Charles University, Faculty of Pharmacy in Hradec Kralove, Akademika Heyrovskeho 1203, Hradec Kralove, 500 05, Czech Republic
[d] Biozentrum, Martin-Luther-University Halle-Wittenberg, Weinbergweg 22, 06120 Halle (Saale), Germany
[e] Fraunhofer Institute for Microstructure of Materials and Systems IMWS, Walter-Hülse-Straße 1, 06120 Halle (Saale), Germany

ARTICLE INFO

Keywords:
Stratum corneum
Liposomes
Ceramides
Skin barrier repairing agents
Langmuir monolayer
Hydrogen bonding network

ABSTRACT

The stratum corneum (SC) is the largest physical barrier of the human body. It protects against physical, chemical and biological damages, and avoids evaporation of water from the deepest skin layers. For its correct functioning, the homeostasis of the SC lipid matrix is fundamental. An alteration of the lipid matrix composition and in particular of its ceramide (CER) fraction can lead to the development of pathologies such as atopic dermatitis and psoriasis. Different studies showed that the direct replenishment of SC lipids on damaged skin had positive effects on the recovery of its barrier properties.

In this work, cerosomes, i.e. liposomes composed of SC lipids, have been successfully prepared in order to investigate the mechanism of interaction with a model SC lipid matrix. The cerosomes contain CER[NP], D-CER [AP], stearic acid and cholesterol. In addition, hydrogenated soybean phospholipids have been added to one of the formulations leading to an increased stability at neutral pH. For the mode of action studies, monolayer models at the air-water interface and on solid support have been deployed. The results indicated that a strong interaction occurred between SC monolayers and the cerosomes. Since both systems were negatively charged, the driving force for the interaction must be based on the ability of CERs head groups to establish intermolecular hydrogen bonding networks that energetically prevailed against the electrostatic repulsion. This work proved for the first time the mode of action by which cerosomes exploit their function as skin barrier repairing agents on the SC.

1. Introduction

The skin is the second largest organ of the human body. Being directly exposed to the external environment, it acts as a physical and chemical barrier and plays a fundamental role in thermal regulation and in preventing water evaporation from basal layers [1,2]. The outermost layer of the skin is called stratum corneum (SC), and it is directly responsible for the protection and permeability of the skin. The structure of the SC can be briefly described as a *brick-and-mortar* system, where the bricks are dead keratinized corneocytes embedded in a dense lipid matrix which acts as the mortar [3–5]. The lipid matrix is composed of an approximately equimolar mixture of ceramides (CERs), cholesterol and free fatty acids (FFA) [6,7]. Mainly CERs are responsible for the SC physical and chemical properties [8,9]. It has been demonstrated that an alteration in the composition of the lipid matrix and in particular variations in the CERs fraction can lead to the generation of chronical diseases such as atopic dermatitis and psoriasis [10–12]. A common approach to treat these pathologies is the replenishment of the missing lipids through topic formulations or by prescribing corticosteroids to treat the local inflammations [10]. Since the delivery of CERs from

Abbreviations: SC, Stratum Corneum; CER, Ceramide; FFA, Free Fatty Acid; LA, Lignoceric Acid; SA, Stearic Acid; CPP, Critical Packing Parameter; PL, Phospholipid; AFM, Atomic Force Microscopy; GIXD, Grazing Incidence X-ray Diffraction; TRXF, Total Reflection X-ray Fluorescence; DLS, Dynamic Light Scattering; TEM, Transmission Electron Microscopy; HbN, Hydrogen bonding Network; LB, Langmuir-Blodgett; LS, Langmuir-Schaefer.

* Corresponding author.
E-mail address: gerald.brezesinski@iadp.eu (G. Brezesinski).

https://doi.org/10.1016/j.bbadva.2021.100039

Available online 26 December 2021

conventional formulations such as ointments and creams is poor, other formulation strategies have been investigated to improve the delivery efficiency and to target the transfer of CERs into deeper layers of the SC [13–15]. In previous studies, it was shown that the administration of CERs in lipid bilayers or in formulations, which are resembling the structure of the lipid matrix was an effective strategy for supplementing the missing CERs in damaged skin models [16,17]. The creation of liposomes or lipid nanoparticles based on skin CERs has been extensively investigated in literature. The main issue of liposomal formulations composed of a large fraction of CERs is related to their physical-chemical properties. CERs consist of a sphingosine moiety, which is linked by an amide bond to a fatty acid moiety, and modifications in the head group and/or in the alkyl chains lead to the creation of different subclasses of CERs (Fig. 1) [18,19]. In order to successfully produce stable liposomes, the critical packing parameter (CPP) should be between 0.7 and 1.0. This parameter is defined as the ratio between the tail volume, V, and the head area A multiplied with the tail length l. A dimensionless number can be calculated: CPP=V/(A•l) [20]. If the amphiphile is fairly symmetrical (CPP ~ 1), it can easily be packed into lamellar phases. In mixtures of amphiphilic molecules having complementary shapes, the value of CPP becomes additive [21]. Since CERs have two long chains and a small head group they possess a value of ~1.2, which does not allow the formulation of liposomes in single component systems [22]. The way to overcome this problem is the use of intelligent designed mixed systems.

CERs-based nanosystems are widely used as models for penetration studies [23], as carriers for the topical delivery of non-steroidal anti-inflammatory drugs [24], as tumour cells sensitizers [25]. CER-based liposome formulations have been also developed for the treatment of various skin diseases proving their potential application as a skin barrier recovery agent [17,26,27]. Although the efficacy of such liposomes was firmly established, none of these studies defined the mode of action through which the liposomes interacted with the SC itself.

Thus, the objective of this work was to develop stable liposomal formulation mainly composed of SC lipids, hereinafter referred to as *cerosomes,* which composition closely resembles the natural SC lipid matrix. We investigated the interaction of the designed cerosomes with a model SC lipid matrix monolayer composed of CER[NP], D-CER[AP], cholesterol and lignoceric acid (LA). The addition of phospholipids (PLs) was studied to test feasible stabilisation of the cerosomes. Cerosome samples were characterized by dynamic light scattering (DLS), zeta-potential and transmission electron microscopy (TEM). The SC monolayer was either deposited onto a liquid surface or onto a functionalized solid surface. The interaction was probed by means of adsorption isotherms after subphase injection, and after the transfer to a solid support by atomic force microscopy (AFM) measurements. Despite the negative electrostatic charge of both the SC model and the cerosome systems, a strong attraction was observed and the nature of the phenomenon will be discussed. Moreover, the characterization of the SC model by X-ray diffraction was made in order to prove its structural resemblance to a native SC lipid matrix.

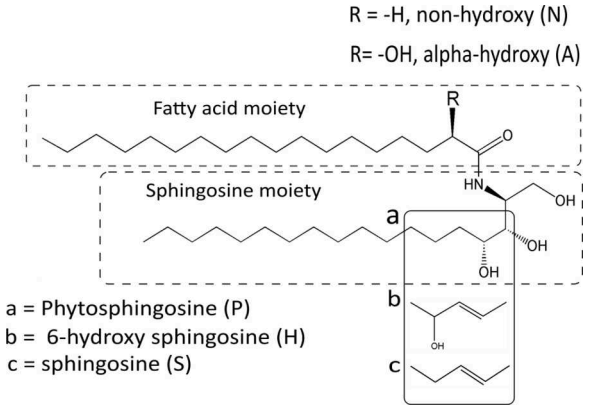

Fig. 1. Chemical structure of human CERs and possible chain and head modifications. The length of the fatty acid moiety can range from C14 to C26 while the sphingosine moiety is between C14 and C18.

2. Experimental section

2.1. Materials

CER[NP]-C24:18 (N-(tetracosanoyl)-phytosphingosine) and D-CER[AP]-C24:18 (N-(2R- hydroxytetracosanoyl)-phytosphingosine) were synthesized and further purified to achieve ≥ 95% purity. Cholesterol (purity ≥ 95%), lignoceric acid (LA) (purity ≥ 99.9%), stearic acid (SA) (purity ≥ 99.5%), dichlorodimethylsilane (purity ≥ 99.5%) and PBS buffer solution at pH 7.4 were purchased from Sigma Aldrich GmbH (Taufkirchen, Germany) and used without further purification. HPLC grade methanol, chloroform (purity ≥ 99.8%), TRIS and NaCl were purchased from VWR International GmbH (Darmstadt, Germany) and used as received. The hydrogenated soybean PLs S75-3 and P100-3 were generously provided by Lipoid GmbH (Ludwigshafen, Germany). CER[NP]-C18:18 (N-(octadecanoyl)-phytosphingosine) and D-CER[AP]-C18:18 (N-(2R-hydroxyoctadecanoyl)-phytosphingosine) were kindly supplied by Evonik Industries AG (Essen, Germany). The compounds were further purified using column chromatography to achieve the highest purity. Millipore water was obtained from Sinergy® apparatus (Merck, Darmstadt, Germany) (resistivity 18 MΩ•cm at 25°C).

2.2. Sample preparation

2.2.1. SC monolayer model

The SC monolayer model was composed of a 1:0.7:1 molar mixture of CERs, cholesterol and lignoceric acid (CERs:Chol:LA). The CERs mixture contained CER[NP] (24:0, 18:0) and D-CER[AP] (24:0, 18:0) in a 2:1 molar ratio. This lipid mixture was dissolved in $CHCl_3$:MeOH (3:1 v:v) to a final concentration of ~1 mg/ml to obtain a SC lipid solution used for the model Langmuir monolayer formation. As subphase, Millipore water was used.

2.2.2. Preparation of liposomes

Liposome solutions of different composition were prepared by the thin layer method [28]. Lipid powder was dissolved in 2:1 (v:v) $CHCl_3$:MeOH solution. To form a thin lipid film on the flask's wall, the solvent was removed by rotary evaporator and further kept in vacuum at 25°C for 24 hours to remove any solvent traces. The dried film was rehydrated with an appropriate buffer at 80°C, well above the lipid mixture melting temperature, and vortexed to form multilamellar vesicles. The multilamellar vesicles were homogenised by extrusion through a polycarbonate membrane filter with pore sizes of 100 nm in diameter (Cytiva, MA, United States) using an Avanti extruder kit (Alabama, United States). The used lipid compositions of studied cerosomes and types of buffer used are listed in Table 2.

2.2.3. Sample preparation for atomic force microscopy (AFM) experiments

Langmuir Blodgett (LB) and Langmuir Schaefer (LS) depositions for AFM experiments were performed using KSV Nima Langmuir trough (Gothenburg, Sweden) equipped with a dipping arm. A LB deposition technique was used to transfer the SC lipid monolayer onto a solid support. The substrate used was a round mica sheet with 25 mm diameter (Micro to Nano, Haarlem, Netherlands). First, a lipid monolayer was formed at the air/water interface on the Langmuir trough apparatus by spreading an appropriate amount of the lipid solution in the volatile solvent and further compression to a target surface pressure of 20 mN/m. Next, the mica support was moved perpendicularly across the air/water interface to achieve a monolayer deposition. The sample was kept in air and was further probed in AFM measurements.

LS deposition method was used to deposit a mixed system composed of the SC model monolayer with adsorbed cerosome vesicles onto a solid substrate. In order to induce surface hydrophobicity, a round glass substrate with a 25 mm diameter (Thermo Fisher Scientific, MA, United States) was functionalized with silica groups following the protocol reported by Tian et al. [29]. As in the case of LB transfer, a lipid monolayer was formed on the air/water interface and compressed to 20 mN/m. Liposome solution was injected into the subphase, and the systems were left for ~60 minutes to equilibrate. The hydrophobic substrate was oriented towards the liquid interface and was lowered parallel to the functionalized air/water interface in order to achieve a transfer of a monolayer decorated with adsorbed vesicles onto the hydrophobic solid support. The system was kept under water using a special sample cell, and further carefully transferred to the AFM apparatus for the structural investigation.

2.3. Grazing-incidence X-ray diffraction (GIXD)

GIXD experiments were performed at the beamline PO8 (Petra III of Deutsches Elektronen-Synchrotron (DESY), Hamburg, Germany). The synchrotron beam was monochromatized by a set of two monochromators (Silicon double crystal (Si 111) and a Germanium double crystal (Ge 311). The photon energy was set to 15 keV (wavelength $\lambda = 0.827$ Å). The Langmuir trough (Riegler & Kirstein, Potsdam, Germany) was placed in a hermetically sealed container, which was constantly flushed with pre-wetted Helium (He). The temperature of the trough was kept at (20 ± 1)°C. The incident beam hits the air/water interface at 0.07° just below the critical angle α_{cr} of total external reflection ($\alpha_{in} = 0.85 \bullet \alpha_{cr}$), such that only the immediate vicinity of the interface is probed. The footprint of the incoming beam on the monolayer surface was approximately 1 × 50 mm^2. The diffraction signal was collected by a vertically-oriented position sensitive (PSD) detector (MYTHEN, microstrip system for time resolved experiments, DECTRIS, Baden, Switzerland). A Soller collimator (JJ X-RAY, Denmark) was placed between the sample and the detector to restrict the in-plane divergence of the diffracted beam to 0.09°. The diffraction data consist of Bragg peaks in the 2-dimensional intensity vs. (Q_{xy}, Q_z) space. The visualization of the diffraction peaks was performed using an in-house written python macro. To obtain the information on the monolayer structure, i.e. chain lattice parameters, tilt angle, distortion, cross-sectional area (A_0) and the in-plane lattice area of one chain (A_{xy}), the collected diffraction peaks were analyzed using a procedure established earlier [30]. The diffracted intensity was integrated over a defined vertical Q_z window and over a horizontal Q_{xy} window to obtain Bragg peaks (I vs. Q_{xy}) and Bragg rods (I vs. Q_z), respectively. These curves were further modelled with 1-dimensional Gaussian functions in Q_z-direction and 1-dimensional Lorentzian functions in Q_{xy}-direction accordingly. The obtained Bragg peak and rod positions and their corresponding full-width at half-maximum (FWHM) allowed to extract information on the monolayer structure. In order to take the in-plane divergence of the X-ray beam into account, the FWHM of the Lorentzian peaks were corrected as follows:

$$FWHM_{xy}^{cor} = \sqrt{\left(FWHM_{xy}^{meas2} - FWHM_{xy}^{res2}\right)^2}, \text{ with } FWHM_{xy}^{res} = 0.0122 \text{Å}^{-1}.$$

The in-plane dimensions of the formed domains were than deduced using the Scherrer equation: $L_{xy} = 0.9 \frac{2\pi}{FWHM_{xy}^{cor}}$

2.4. Liposome characterization

2.4.1. Dynamic light scattering

The size distribution of the liposome formulations was characterized by DLS with a Zetasizer Nano ZS device (Malvern Instruments, Worcestershire, UK). The measurements were performed at 25°C using polystyrene disposable cuvettes (Roth, Karlsruhe, Germany). Each measurement was repeated three times on the same sample with 15 runs per measurement. In the cuvette, the solution was composed of 0.9 mL of buffer and 0.1 mL of liposome suspension. The samples were measured immediately after the preparation, and once per week during the following three weeks. In the meantime, the samples were stored at ~5°C in dark environment.

2.4.2. Zeta-potential

Zeta potential measurements were performed with the Zetasizer Nano ZS device (Malvern Instruments, Worcestershire, UK). Disposable cuvettes were equipped with a platinum electrode. By using buffer of the appropriate composition, the conductivity of the solutions was kept under the value of 2 mS/cm to avoid the formation of bubbles in the sample cell which could modify the electrophoretic mobility of the liposomes. Each measurement was repeated three times on the same sample with a number of runs selected automatically by the software.

2.4.3. Transmission Electron Microscopy (TEM)

To prepare TEM-samples, 3 μl of the dispersion were spread onto a Cu-grids coated with a formvar film. After 1 min of adsorption, excess liquid was blotted off with filter paper. Subsequently, the grids were air-dried for 10 seconds, washed with water (3 times for 1 minute), placed on a droplet of 2% aqueous uranyl acetate and drained off after 1 min. The dried specimens were examined with an EM 900 transmission electron microscope (Carl Zeiss Microscopy, Jena, Germany) at an acceleration voltage of 80 kV. Electron micrographs were taken with a Variospeed SSCCD camera SM-1k-120 (TRS, Moorenweis, Germany). TEM micrographs were taken immediately after liposomes preparation.

2.5. Interaction studies

2.5.1. Subphase injection

An experimental setup consisting of a perfluorether Petri dish and a Wilhelmy balance was used to record the variation of the surface pressure over time (ΔΠ vs. t). The Petri dish had a diameter of 5.5 cm and a depth of 0.5 cm with a total area of 23.8 cm^2. The setup allowed to probe the interaction between a pre-formed monolayer and a surface-active formulation injected directly into the subphase by inserting a syringe needle vertically through the lipid film to minimize any layer perturbations. A liposomes solution was injected underneath the pre-formed monolayer with a surface pressure of 20 mN/m, the final liposome concentration was of 0.025 mg/ml. The variation of surface pressure, ΔΠ, over time, t, was recorded. No stirring was applied, and the measurement was started right after the injection.

2.5.2. AFM measurements

Atomic force microscopy (AFM, NanoWizard IV, JPK Instruments/ Bruker, Berlin) in Quantitative Imaging Mode (QI) was performed to investigate the surface roughness and topography. Topographical images were recorded in liquid state using silicon cantilever (qp-BioT, Nanosensors) in a standard liquid cell (JPK Instruments) containing the needed buffer. Post processing and roughness analysis were performed using the software JKP Data Processing V5.0.85 (JPK Instruments, Berlin, Germany) and Gwyddion V2.9 (Gwyddion, open source). The software Fiji/ ImageJ (Fiji, open source) was used for calculating the areas of each domain in AFM micrographs.

3. Results and discussion

3.1. SC monolayer characterization by GIXD

The objective of this paper was to study and clarify the mode of action of liposomes made of SC lipids, so-called cerosomes, with a 2D model of the SC lipid matrix. First, the used SC model monolayer (composition in section 2.2.1) was characterized in detail. The lipids used in this model had C24 long chains since the native SC lipids possess

mainly chains between C22 and C26 length [18,19]. The experimental isotherm of the SC model mixture was recorded at different temperatures [31] and corresponds to a classical condensed monolayer with no additional phase transitions except the transition from the gas-analogous phase (GS) to the liquid-condensed phase (LC) at nearly zero surface pressure. The model used in this work was already partly studied as Langmuir monolayers and by neutron diffraction with results similar to the native SC lipid matrix [31,32]. However, these methods did not give information regarding the lateral structure of the model. Thus, Grazing Incidence X-ray Diffraction (GIXD) has been applied to study the lateral structure of our SC model monolayer and compared it to the structure of native SC.

GIXD measurements on a SC model monolayer at high lateral pressure (30 mN/m) revealed the presence of four distinct diffraction peaks all located at the horizon ($Q_z = 0$) (Fig. 2a). A closer inspection of the positions of the emerged Bragg peaks allowed to deduce the presence of two separated lattices. Two peaks centred at 1.45 $Å^{-1}$ and 1.63 $Å^{-1}$ can be attributed to the phase 1 with ordered chains exhibiting a cross-sectional area of 20.2 $Å^2$, typical for the rotator phase (free rotation of the chains) in PL monolayers [33]. The other two remaining Bragg peaks located at 1.50 $Å^{-1}$ and 1.67 $Å^{-1}$ were assigned to the phase 2 with tightly packed chains of a cross-sectional area of 19.0 $Å^2$, typical for a highly ordered 2D crystalline phase [33]. The chains in each phase were arranged in an orthorhombic unit cell, the typical lateral structure of the SC lipid matrix [34–36]. The obtained diffraction data along with the deduced structural parameters of the model SC monolayer are summarised in table 1.

The correlation length estimated by using the Scherrer formula (section 2.3) was 314 / 314 Å and 35 / 64 Å for the phase 2 and phase 1, respectively. These values indicated that the monolayer areas of phase 2 were much more homogenous with low number of defects, in contrast to phase 1 comprising relatively small condensed domains with many defects.

The diffraction peaks attributed to the orthorhombic structure of phase 2 of our model SC monolayer were located at similar positions as the peaks found in WAXS measurements with bulk dispersion of human SC lipids [35]. However, the composition of the two phases and the origin of the second orthorhombic lattice attributed to phase 1 remained unclear. But considering that the lipids must arrange in a hairpin configuration in monolayers at the air-water interface while in native SC the CERs arrange preferably in a fully extended configuration [37], phase separation into different mixtures in this 4 component systems is easily imaginable. However, the proposed SC monolayer model can still serve as a consistent and reliable model system regarding surface interactions.

Table 1
Peak positions ($Q_{xy} \pm 0.003$ $Å^{-1}$ and $Q_z \pm 0.005$ $Å^{-1}$), lattice parameters of the unit cell (a, b, c, and α, β, γ), tilt angle (t), cross-sectional area ($A_o \pm 0.1$ $Å^2$), and in-plane chain area ($A_{xy} \pm 0.1$ $Å^2$) extracted from GIXD data of a SC model monolayer at 30 mN/m on a water subphase at 20°C.

	Q_{xy}^1/Q_z^1 ($Å^{-1}$)	Q_{xy}^2/Q_z^2 ($Å^{-1}$)	a/b/c (Å)	α/β/γ (°)	t (°)	A_0 ($Å^2$)
SC	1.45	1.63	5.239	116.6	0	20.2
Phase 1	0	0	4.661 4.661	124.2 124.2		
SC	1.50	1.67	5.042	112.3	0	19.0
Phase 2	0	0	4.529 4.529	123.8 123.8		

Additionally, lignoceric acid, CER[NP] (24:0, 18:0) and D-CER[AP] (24:0, 18:0) have been measured as single-component systems (Fig. S1), and the corresponding monolayer structures are discussed in the supporting information.

Simultaneously with GIXD, Total Reflection X-ray Fluorescence (TRXF) experiments were carried out on the same model SC monolayer to determine its charge state at neutral pH. TRXF allows to quantify ion adsorption at the air/water interface [38,39] and thus to measure electrostatic interactions between counterions (anions or cations) and a charged (or even uncharged) monolayer. A 5 mM $ZnCl_2$ solution at pH 7 was used as subphase in order to determine any counterion excess at the surface. The comparison of the recorded fluorescence signal from the bare interface and from a SC model monolayer on the same subphase (Fig. S2) demonstrated a strong enrichment of zinc cations near the monolayer, which implies that the SC monolayer possess a negative charge at pH 7.

The characterization of the SC model was also performed in multilayer systems. Two co-existing lamellar phases plus a small amount of phase-separated cholesterol have been detected (Fig. S3). Interestingly,

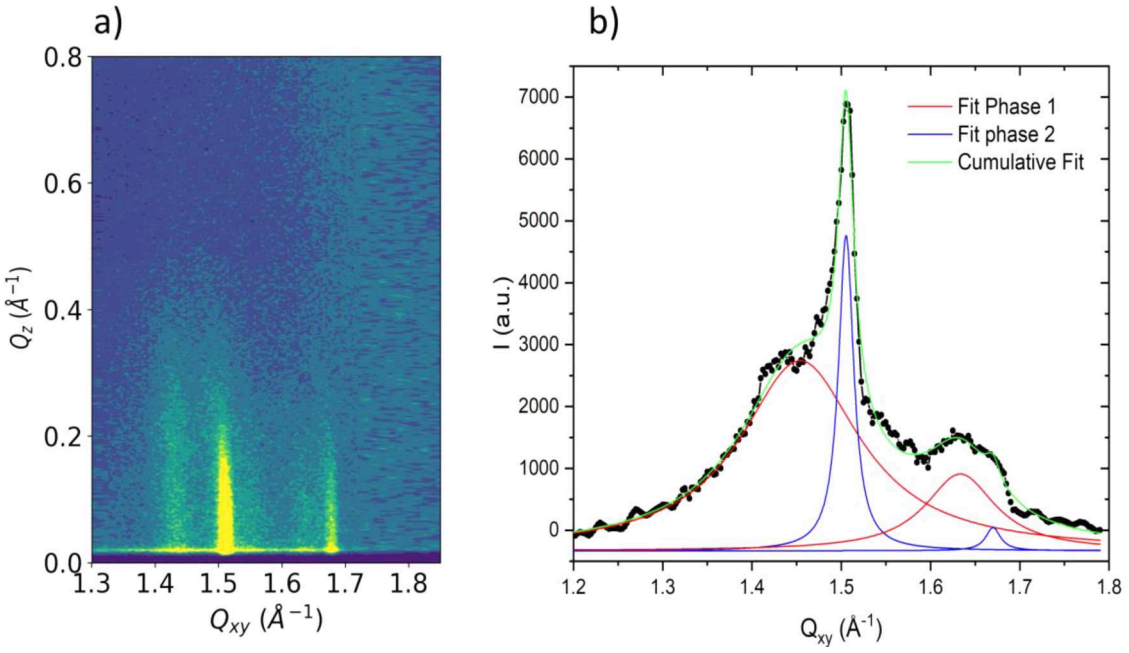

Fig. 2. a) Contour plot of the scattered X-ray intensity as a function of the in-plane component (Q_{xy}) and the out-of-plane component (Q_z) of the scattering vector of model SC monolayer, b) fitting of Bragg peaks (I vs. Q_{xy}) by Lorentzian functions.

one lamellar phase exhibited an orthorhombic in-plane unit cell with high packing density ($A_0 = 18.8$ Å^2). The second phase is not seen in the WAXS scattering profile most probably because a liquid-ordered phase has been formed in the aqueous dispersion instead of the rotator phase observed in the monolayer. The detailed results will be only discussed in the supporting information.

3.2. Liposome formulations

In the next step, the development of stable SC liposomes, so-called *cerosomes*, was carried out. Since CERs with a CPP of ~1.2 cannot form stable liposomes in single-component systems, a first formulation was composed of CER[NP], D-CER[AP] (both with symmetric alkyl chains (18:0, 18:0)), cholesterol and SA and mixed in the desired final ratio (table 2). The additive packing parameter calculated for this mixture is ~0.95 which ranges between 0.75 and 1, the value reported for liposome formation [21]. Additionally, this composition was chosen to produce liposomes which resemble the SC lipid matrix [40,41]. In previous studies, it has been shown that CER[NP] when used as single CER in a SC model system tends to phase segregate creating CER crystals [17,42], the addition of D-CER[AP] prohibits such phenomena forming instead homogenous vesicles. Nevertheless, it was shown that formulations based on similar SC lipid mixtures featured poor long term stability due to the high rigidity of the vesicles [23,43].

To overcome this issue, hydrogenated soybean PLs have been added to the above described cerosome composition. The added PLs acted as a stabilizing agent (table 2) since phosphatidylcholines exhibit also a favourable CPP of ~0.9 [22,44]. The calculated additive packing parameter for this new mixture was ~0.9. Two plant-based PLs called S75-3 and P100-3 were selected to be incorporated into the cerosome formulation. The first number refers to the relative percentage of phosphatidylcholine in the mixture, i.e. either 75% or 100%, accordingly, the -3 indicates hydrogenated chains and the letter refers to the extraction source (S for soybean and P for non-GMO soybean). Although PLs are not present in the native SC lipid matrix, toxicity studies of PL based microemulsions and liposomes on the human skin proved a very low toxicity potential of these components, therefore making them harmless for their incorporation into the studied liposomes [45].

3.2.1. Cerosome characterization

First formulation developed and characterized was the cerosome formulation composed of only SC lipids. The method selected for homogenizing the particle size of our liposomes was the extrusion method via 100 nm filter. At neutral pH, the cerosomes demonstrated the expected stability problem as rapid formation of aggregates occurred [23].

An increase of the subphase pH to 10 allowed to electrostatically stabilize the liposomes by increasing the ionization state of SA molecules and to obtain stable and reproducible liposome samples [46]. The extruded cerosomes exhibited a polydispersity index (PdI) of 0.27 presenting two populations of liposomes, a small and predominant one with diameter of ~130 nm and a second one with larger diameter of ~850 nm, while the measured zeta-potential was -35.5 mV indicating a noticeable negative charge of the sample [47]. The aging of the formulation was tested over a period of three weeks, as shown in Fig. 3. The PdI of the cerosomes increased from 0.27 to 0.36 which indicated that the liposomes aggregated and flocculated proving the presence of structural instability in the formulation. The TEM micrograph of the extruded sample (Fig. 4a) confirmed the presence of smaller and larger vesicles proving the formation of liposomes.

3.2.2. Cerosome/Phospholipid characterization

Since the skin surface possesses an average pH of 5 [48], the use of topic formulations with basic pH may have negative impact on the skin [49]. As previously discussed, the cerosome formulation composed of only SC lipids was not stable at physiological pH. To solve this problem, hydrogenated soybean PLs S75-3 and P100-3 were tested as stabilizing agents for the incorporation in a second cerosome formulation (table 2). To test their potential incorporation into the cerosome, lecithin vesicles were as well prepared by extrusion via 100 nm diameter filters and were investigated by DLS and zeta potential at neutral pH to test their properties.

Liposomes made of P100-3 had a large PDI of 0.37 and started to flocculate and precipitate after few days. S75-3 liposomes showed a lower PDI of 0.16 indicating the formation of more homogenous vesicles moreover, this exhibited a negative charge almost three times higher than P100-3 (-15.5 mV vs. -5.7 mV). The TEM micrograph (Fig. 4 c and d) confirms vesicle formation with small size distribution. These properties together with the higher stability were the determining factors for the selection of the S75-3 for use in model cerosomes.

The cerosome containing S75-3 had shown several advantages in comparison to the phospholipid-free formulations. Importantly, stable liposomes were formed in PBS buffer at pH 7.4. A PdI of 0.08 was obtained showing a single vesicle population with diameter of ~130 nm proved by the TEM image (Fig. 4b). The measured zeta-potential of -33 mV indicated a high enough charge of the vesicles at pH 7.4 for

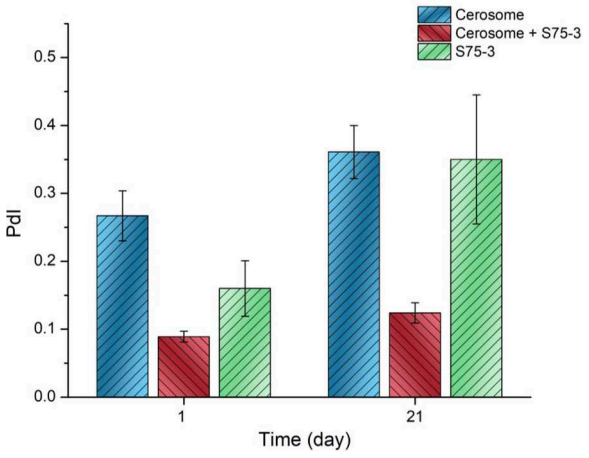

Fig. 3. Stability analysis of vesicle formulations presented as polydispersity index (PdI) versus time.

Table 2
Compositions of the tested extruded formulations. Each sample was prepared to obtain a final concentration of 1 mg/ml in the respective aqueous solution. The lipid content is relative to the molar ratio in each mixture. PdI and all size and zeta-potential measurements were performed at 25°C.

	Aqueous solution	CER[NP]	D-CER[AP]	Chol	SA	PL	PdI	ζ-pot(mV)
Cerosome	100 mM NaCl 10 mM TRIS, pH 10	0.66	0.33	0.7	1	-	0.27 ± 0.06	-35.5 ± 2.1
Cerosome + S75-3	PBS, pH 7.4	0.66	0.33	0.7	1	1	0.08 ± 0.01	-33.4 ± 2.4
S75-3	PBS, pH 7.4	-	-	-	-	1	0.16 ± 0.04	-15.5 ± 1.3
P100-3	PBS, pH 7.4	-	-	-	-	1	0.37 ± 0.1	-5.7 ± 0.8

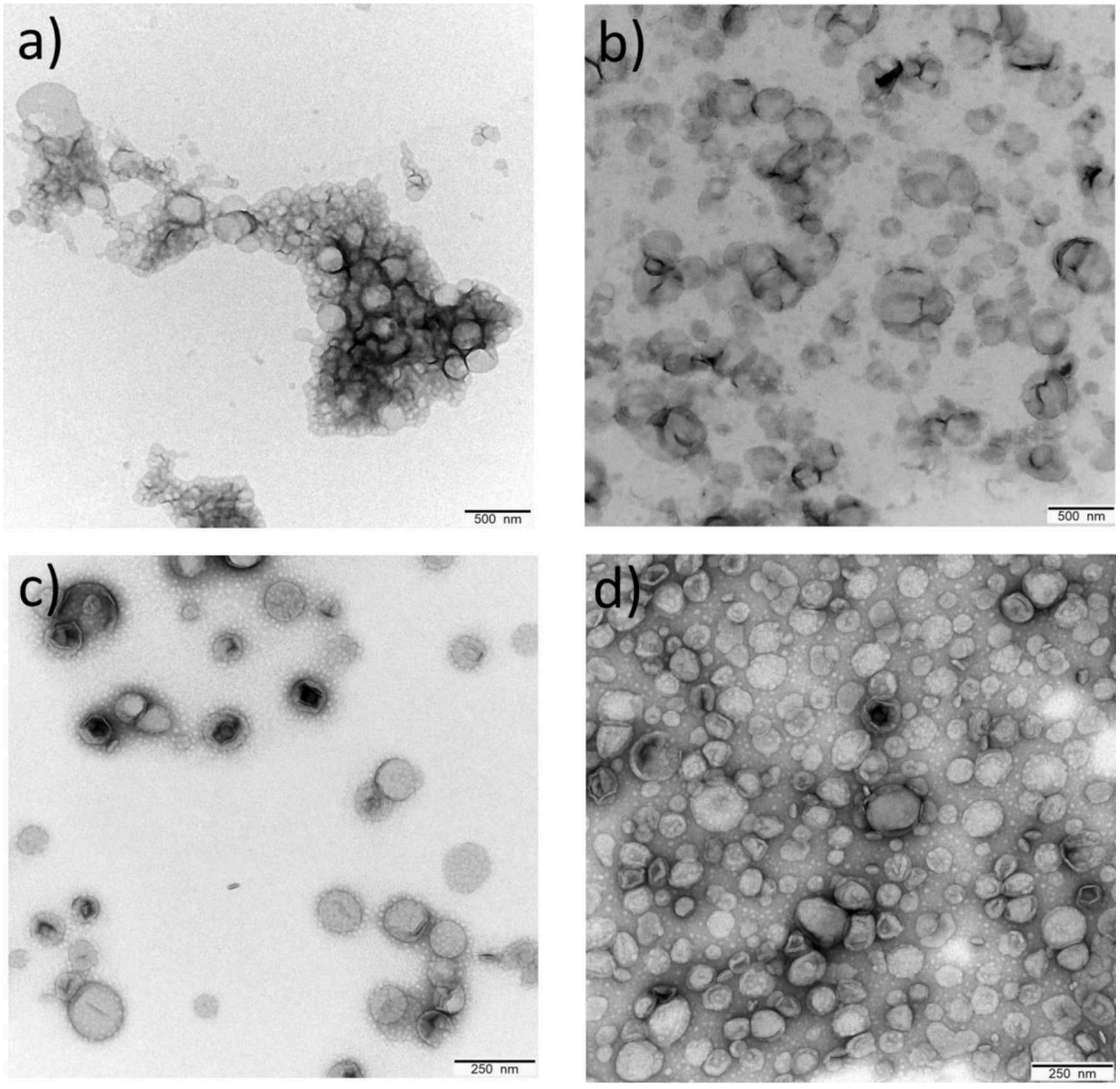

Fig. 4. TEM images by negative staining of a) Cerosome, b) Cerosome + S75-3, c) P100-3 and d) S75-3.

electrostatic stabilization. Stability analysis of the formulation showed that after three weeks the PdI of the sample increased only slightly to 0.12 (Fig. 3) showing a high sample stability with no vesicles aggregation over time. These results confirmed that the addition of S75-3 into the cerosomes allowed the generation of a stable at physiological pH sample with a high negative charge.

3.3. Mode of action studies

3.3.1. Adsorption experiments

Once the cerosome formulations have been developed and characterized, the interaction between these and monolayers of the SC lipid matrix model was investigated. Monolayers are effective model systems to study the physical-chemical properties of amphiphiles and their interaction with colloidal systems [50,51]. The SC model mixture selected to interact with the cerosomes was the one previously characterized by X-ray scattering methods which proved to effectively reproduce structural properties typical of native SC.

The first method of choice used to characterize the interaction between the two systems was the so-called subphase injection method. The extruded liposome formulations have been injected underneath a preformed SC model monolayer with an initial surface pressure of 20 mN/m directly into the subphase. The surface pressure of 20 mN/m has been selected because of stability reasons. Different monolayer experiments showed that the packing density and structure is practically the same at 20 and 30 mN/m. The subphases used for such experiments consisted of the solutions used for preparing the different liposomal formulations (table 2).

The cerosome formulations with and without S75-3 resulted in a surface pressure variation ($\Delta\Pi$) of (24.6 ± 2.1) mN/m and (23.4 ± 2.4) mN/m, respectively (Fig. 5a), showing high affinity towards the SC model monolayer. Fig. 5b displays the kinetics curves of adsorption of the vesicles at the monolayer with a plateau (equilibrium state) reached after ~60 minutes for each formulation. Besides the cerosome formulations, the PLs vesicles were also tested for their ability to be adsorbed at the SC model monolayer. In comparison to the cerosomes, a significantly lower $\Delta\Pi$ was registered with S75-3 (7.4 ± 1.1 mN/m) and P100-3 (3.5 ± 0.8 mN/m) (Fig. 5a) proving that liposomes with a composition resembling the SC lipid matrix were necessary to establish strong interactions with the SC model monolayer.

The strong affinity between the cerosomes and the SC model monolayer was remarkable, as both systems were negatively charged at neutral pH suggesting that electrostatic repulsion may prevail. But instead of electrostatic repulsion strong interaction was observed.

The interaction between equally charged layers is a long-standing argument. The most obvious explanation is the attraction between two like-charged surfaces mediated by divalent ions. The interfacial water reacts to the presence of surface charges, and the restructuring modifies

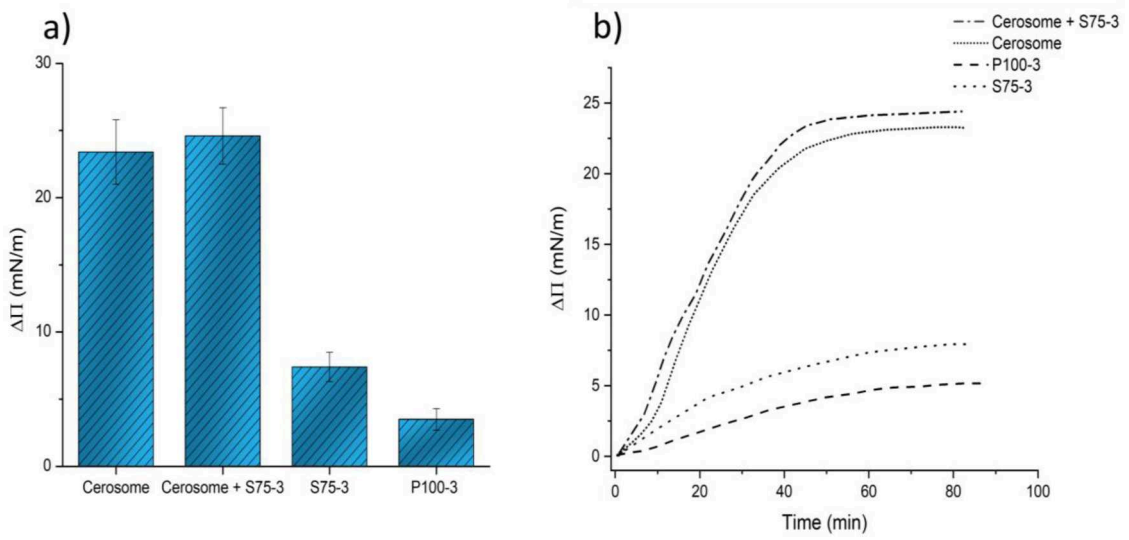

Fig. 5. a) Maximum variation of surface pressure, ΔΠ, from the initial surface pressure value of 20 mN/m after injection of vesicle formulations, b) ΔΠ versus time kinetics of adsorption of liposomes. Each injection experiment was performed in a subphase with the same aqueous solution used for the formation of each liposome formulation.

the surface interaction and leads to like-charge attraction resulting from counterion-correlation enhanced by a decrease of the water dielectric constant in confinement [52]. The dielectric constant of interfacial water has been predicted to be smaller than that of bulk water because of the decrease of the rotational freedom of water dipoles near surfaces. [53]. But also electrostatic interactions between highly charged double bilayers in the presence of monovalent counterions and in strong confinement have been investigated. Attractive electrostatic interactions, which are in contradiction to continuous theories, have been demonstrated [54]. For the present case, the most important finding is that observed for glycolipids [55]. The cross-linking ability of glycolipids promotes membrane adhesion via the formation of saccharide bonds. Some of these head groups were even able to bind adjacent membranes together against the repulsive forces generated by introduced negatively charged PLs. Additionally, cholesterol might reduce the interbilayer separation distance depending on the cholesterol concentration in the bilayer. Cholesterol spreads the lipid molecules in the plane of the bilayer allowing the PL head groups from apposing bilayers to interpenetrate as the bilayers are squeezed together [56].

As showed in Fig. 6, strong head group interactions between the CERs in the monolayer and in the liposomes could be the main reason to overcome the electrostatic repulsion due to negatively charged fatty acids. CERs head groups are well known to form intermolecular hydrogen bonding networks (HbN). The HbN in the SC lipid matrix is fundamental for the stabilization and formation of dense lateral packing (orthorhombic unit cell) within the lipid matrix [34–36]. Studies performed with the single CER[NP] and D-CER[AP] showed convincingly that these CERs were able to establish such HbN [57–59]. Since both

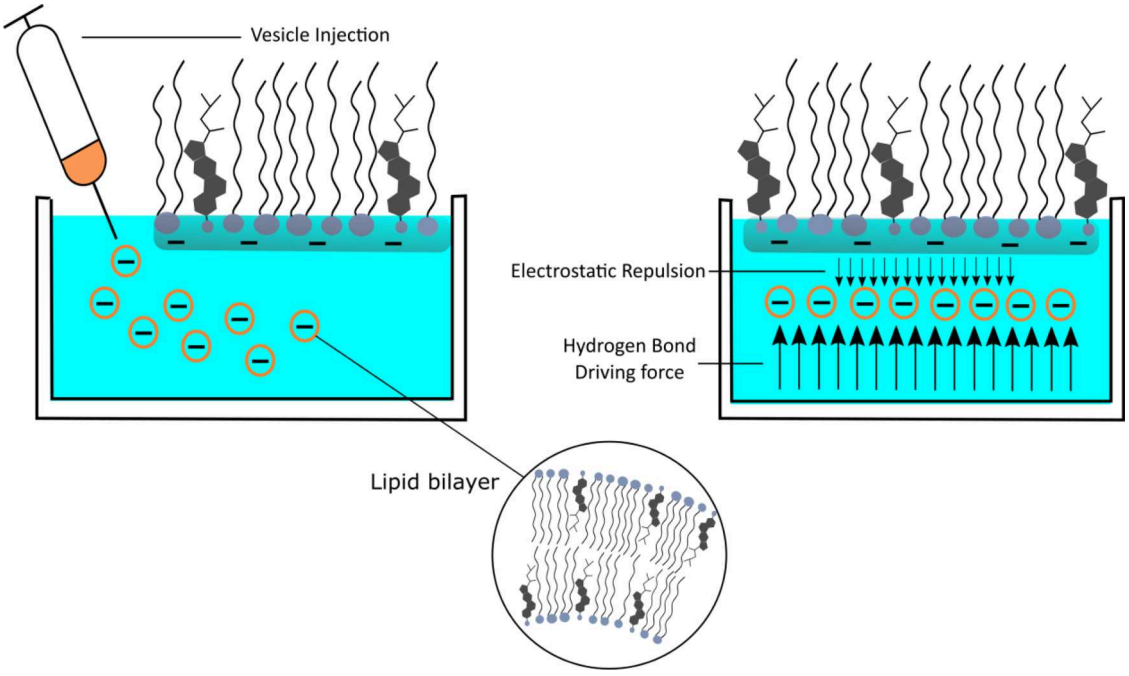

Fig. 6. Schematic representation of cerosome injection underneath a pre-formed SC model monolayer (left) and presentation of the interaction types with vesicle adsorption driven by hydrogen bonding forces between CERs (right).

systems possess these CERs, it is highly plausible to assume that the intermolecular HbN was the driving force which allowed the cerosomes to be adsorbed at the SC model monolayer overcoming the electrostatic repulsion forces (Fig. 6). Local fluctuations might drive the cerosomes close enough to the monolayer to create HbN not only within the layers but also between the layers. The locally formed HbN must be stronger than the electrostatic repulsion to attract more cerosomes to the monolayer surface. This assumption was also supported by the results obtained with the phospholipid liposomes. Since only a weak interaction has been observed in injection experiments (Fig. 5), the formation of a feeble HbN or its complete absence could be presumed. Therefore, phospholipid liposomes have much lower affinity towards the SC model monolayer.

3.3.2. *AFM experiments*

Although the adsorption experiments using Langmuir monolayers provided the direct evidence of the strong attractive interaction between the studied systems, the information about the structures of the formed assemblies was still missing. Several options are imaginable: the cerosomes could get adsorbed underneath the monolayer as intact vesicles, or by reaching the critical coverage concentration could break and form a bilayer or a multilayer. In addition, the lipids may penetrate into lipid-free defects of the SC model monolayer. To deduce the most plausible scenario, AFM experiments were performed. This technique allows to resolve the lateral organization and to visualize the presence of lipid domains and/or adsorbed vesicles by performing topographic surface measurements of the sample deposited onto a solid support with an Angstrom resolution in transversal direction.

AFM experiments in air were carried out on a SC model monolayer transferred onto a mica substrate (see section 2.2.3). The sample deposition was performed at the same monolayer surface pressure of 20 mN/m as the adsorption experiments. The recorded AFM topographic images showed the existence of two types of distinct domains (Fig. 7a). The main domain with a height of 2.4 - 2.6 nm occupied ~70% of the total surface, and a lower 1 - 1.2 nm domain could be additionally distinguished.

In other comparable AFM experiments performed with simple SC monolayers [60,61] the higher domain was defined as the FFA-rich domain were the LA and the CERs were oriented in a hairpin configuration organized in an orthorhombic structure. Differently, the lower domain found in other SC monolayers was said to consist of FFA-cholesterol with height difference of 0.7 - 1.2 nm to the higher phase while in our experiments the height difference between the two domains was 1.2 - 1.4 nm. The formation of the low domains could be explained by the inability of certain lipids to reside in the upright state.

After the characterization of the SC monolayer, AFM scans of the SC monolayer plus the adsorbed cerosome formulations were performed. For transferring such systems, the LS method with a hydrophobic

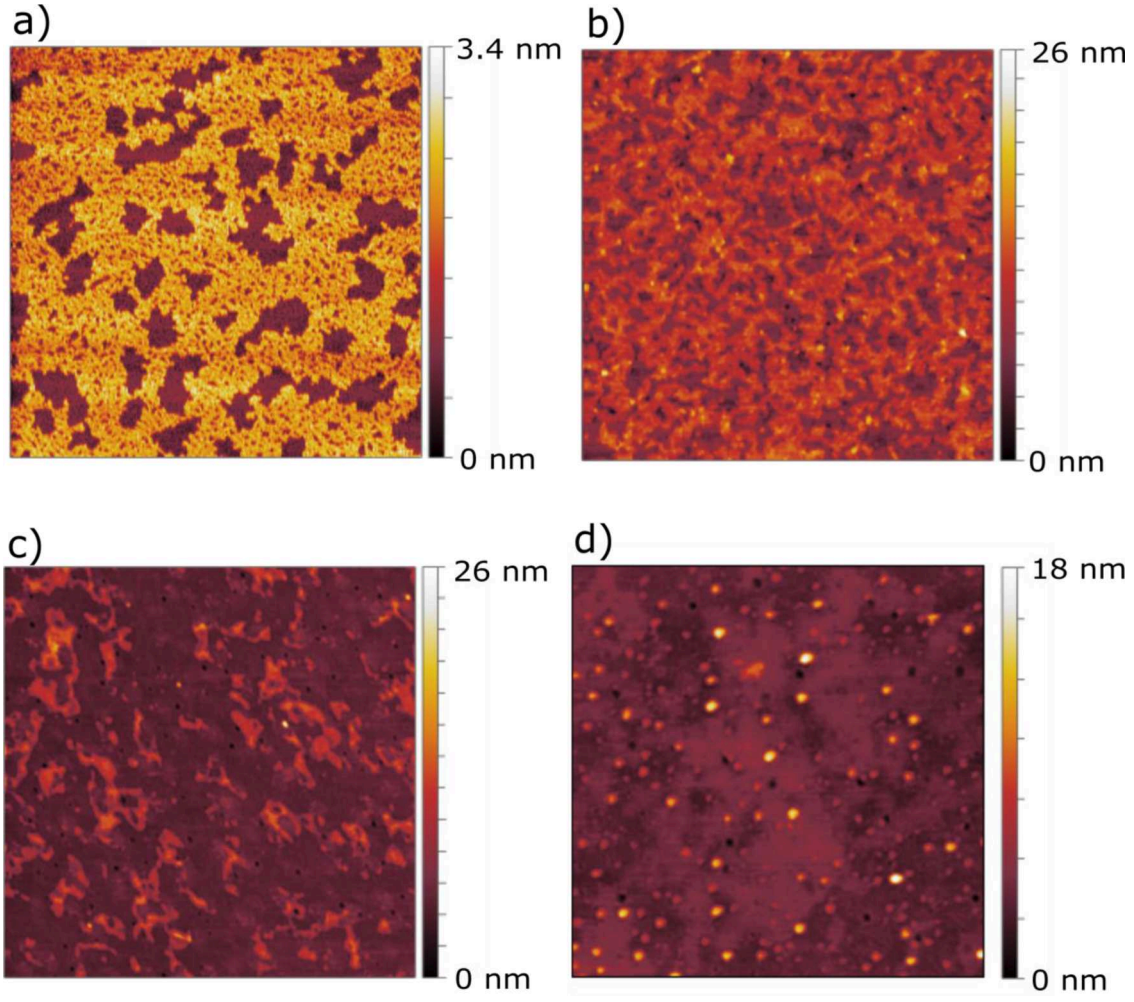

Fig. 7. AFM scans of a) SC model monolayer transferred via LB method onto mica support, b) SC model monolayer after injection of cerosomes, c) SC model monolayer after injection of cerosome + S75-3 formulation, and d) SC model monolayer after injection of S75-3 liposomal formulation. All samples were transferred via the LS method onto glass substrate. Each experiment was performed at 20°C and the subphase used for a) was Millipore water while for b), c), and d) the same aqueous solutions have been used as for the formulation of the liposomes.

substrate was used (see section 2.2.3). In both experiments (Fig. 7b and 7c), adsorption and penetration of lipids from the cerosome formulations into the monolayer was successfully demonstrated, as already suggested by the adsorption experiments. The penetration of the vesicles was deduced from the almost complete disappearance of the 1 nm domains, while the adsorption was deduced from the formation of lipid multilayers as showed by the presence of several nm thick domains (Table S3). For the cerosome formulation without lecithin (Fig. 7b), the adsorbed vesicles spread homogenously over the SC monolayer creating a main domain with height of 8 - 11 nm and ~45% coverage. Other domains with height between 5 - 6 nm (~25 % coverage), 6 - 8 nm (~20 % coverage) and >11 nm with spikes up to 17 nm (~10 % coverage) were observed. Differently, the cerosomes formulated with the S75-3 lecithin formed at the SC model monolayer a main domain with height of 5 - 6 nm (~70 % coverage), and as well domains with height of 6 - 8 nm (~10 % coverage), 8 - 10 nm (~10% coverage) and > 10 nm with spikes up to 22 nm (~10 % coverage).

Finally, AFM scans of the SC model monolayer plus the adsorbed S75-3 liposomal formulation was performed (Fig. 7d). The PLs liposomes, as proven in section 3.3.1, adsorbed at the SC model monolayer, however, not as strong as the cerosome formulations. This difference was also proven in AFM experiments showing that the PLs adsorbed at the SC model monolayer forming a main domain of 3 - 5 nm height and presenting small portions of higher domains with spikes of 15 nm.

The slightly different behavior of the formulation with and without PL might be connected to their composition (table 2). The addition of S75-3 improved the overall stability of the cerosome formulation, and in adsorption experiments a comparable to the phospholipid-free formulation variation of $\Delta\Pi$ was observed. In AFM experiments, both formulations showed a clear adsorption at and penetration into the SC model monolayer. However, smaller domains were formed in formulations with the PL in comparison to the pure cerosomes. Since the PLs constitutes 1/4 of the overall composition of the formulation, it was plausible that the PL fraction decreased the overall adsorption at the SC monolayer forming lipid multilayer domain with lower height.

In addition, quartz-crystal microbalance with dissipation monitoring (QCM-D) experiments were performed to monitor SC model monolayer formation via vesicle fusion on a hydrophobic polystyrene-coated (PS) sensor and to probe the interaction of SC liposomes with such a model SC monolayer. The formation of an almost perfect SC model monolayer on a hydrophobic substrate has been demonstrated. The adsorption of cerosomes onto such a SC model monolayer leads to clearly more material than a monolayer in agreement with the AFM results. The detailed results are discussed in the supporting information (Fig. S4 and S5).

4. Conclusion

Cerosomes or stratum corneum liposomes are a relatively new class of liposomes which are being investigated for the application as skin barrier repairing agents in chronical skin diseases. The aim of this study was to produce stable and reproducible cerosomes and to study their mode of action with SC models. Stable cerosome formulations were obtained using CER[NP], D-CER[AP], cholesterol and stearic acid. However, such formulation presented at physiological pH poor long-term stability due to the high rigidity and low charge density of the vesicles. Higher stability was achieved around pH 10 where an electrostatic stabilization of the vesicles occurs. The addition of the hydrogenated soybean phospholipid S75-3 allowed the production of stable vesicles at physiological pH showing ideal characteristics in terms of particle size distribution and stability over 3 weeks.

Mode of action studies between cerosomes and a SC *in-vitro* model based on monolayers at the air-water interface and later transferred onto solid support proved a high affinity between the two systems. Since both systems, as shown in additional experiments, exhibited a negative surface charge, we deduced that the driving force for the adsorption of the cerosomes at the SC model monolayer was based on the ability of the ceramides head groups, present in both systems, to form intermolecular hydrogen bonding interactions which naturally occur as well in the SC lipid matrix. Moreover, results obtained with the application of AFM showed that the liposomes were able to both penetrate into empty spaces and lower domains present in SC model monolayer and get adsorbed at the monolayer forming localized multilayers.

With the use of simple *in-vitro* models and of suitable methods, we were able for the first time to observe the mode of action by which the cerosomes exploit their function as skin barrier repairing agents on the SC. The use of such formulations might not only be limited to restore the damaged skin but they could be also used to deliver active pharmaceutical ingredients encapsulated in the cerosomes. This might open new and interesting scenarios for treating skin conditions such as inflammations caused by atopic dermatitis and/or psoriasis.

CRediT authorship contribution statement

Fabio Strati: Conceptualization, Methodology, Validation, Investigation, Data curation, Formal analysis, Writing – original draft, Writing – review & editing, Visualization. **Tetiana Mukhina:** Investigation, Formal analysis, Methodology. **Reinhard H.H. Neubert:** Conceptualization, Supervision, Project administration, Funding acquisition. **Lukas Opalka:** Resources, Methodology. **Gerd Hause:** Investigation. **Christian E.H. Schmelzer:** Writing – review & editing. **Matthias Menzel:** Investigation. **Gerald Brezesinski:** Conceptualization, Writing – review & editing, Supervision, Investigation, Formal analysis, Project administration.

Declaration of interests

The authors declare that they have no known competing financial interests or personal relationships that could have appeared to influence the work reported in this paper.

Acknowledgment

This study was funded by the federal state of Saxony-Anhalt through the European Regional Development Fund (ERDF 2014-2020). Dr. Mukhina thanks the German Research Foundation (DFG) (Grant: SCHN 1396/2 ƁLinK``) for the financial support. Dr. Opalka thanks the Czech Science Foundation (19-09600S) for the financial support. Prof. Brezesinski, Prof. Neubert, and F. Strati thank the Phospholipid Research Center Heidelberg for funding (RNE-2019-069/2-1). We thank Prof. Thurn-Albrecht and Dr. Petzold from the physics department in the Martin Luther University Halle-Wittenberg for the access and help with the SAXS/WAXS device. We finally thank the Deutsches Elektronen-Synchrotron (DESY) for beam-time allocation and the team of beamline P08 for support and valuable help.

Supplementary materials

Supplementary material associated with this article can be found, in the online version, at doi:10.1016/j.bbadva.2021.100039.

References

[1] E. Proksch, J.M. Brandner, J.M. Jensen, The skin: An indispensable barrier, Exp. Dermatol. 17 (2008) 1063–1072, https://doi.org/10.1111/j.1600-0625.2008.00786.x.
[2] K.C. Madison, Barrier function of the skin: "La Raison d'Être" of the epidermis, J. Invest. Dermatol. 121 (2003) 231–241, https://doi.org/10.1046/j.1523-1747.2003.12359.x.
[3] L.M. Menon, G K, GW Cleary, The structure and function of the stratum corneum, Int J Pharm 435 (2012) 3–9, https://doi.org/10.1016/j.ijpharm.2012.06.005.
[4] K.A. Walters, M. Dekker, Dermatological and Transdermal Formulations, 2002. https://doi.org/10.1201/9780824743239.
[5] K.A. Holbrook, G.F. Odland, Regional differences in the thickness (cell layers) of the human stratum corneum: an ultrastructural analysis, J. Invest. Dermatol. 62 (1974) 415–422, https://doi.org/10.1111/1523-1747.ep12701670.

[6] M.A. Lampe, A.L. Burlingame, J. Whitney, M.L. Williams, B.E. Brown, E. Roitman, P.M. Elias, Human stratum corneum lipids: characterization and regional variations, J. Lipid Res. 24 (1983) 120–130. http://www.ncbi.nlm.nih.gov/pubmed/6833889.

[7] A. Weerheim, M. Ponec, Determination of stratum corneum lipid profile by tape stripping in combination with high-performance thin-layer chromatography, Arch. Dermatol. Res. 293 (2001) 191–199.

[8] P.M. Elias, K.R. Feingold, M. Mao-qiang, P.M. Elias, K.R. Feingold, Fatty acids are required for epidermal permeability barrier function . Fatty Acids Are Required for Epidermal Permeability Barrier Function, J. Clin. Invest. 92 (1993) 791–798.

[9] A. Schroeter, M.A. Kiselev, T. Hauß, S. Dante, R.H.H. Neubert, Evidence of free fatty acid interdigitation in stratum corneum model membranes based on ceramide [AP] by deuterium labelling, BBA - Biomembr 1788 (2009) 2194–2203, https://doi.org/10.1016/j.bbamem.2009.07.024.

[10] F.F. Sahle, T. Gebre-Mariam, B. Dobner, J. Wohlrab, R.H.H. Neubert, Skin diseases associated with the depletion of stratum corneum lipids and stratum corneum lipid substitution therapy, Skin Pharmacol. Physiol. 28 (2015) 42–55, https://doi.org/10.1159/000360009.

[11] A. Imokawa, G. Abe, A. Jin, K. Higaki, Y. Kawashima, M. Hidano, Decreased level of Ceramides in Stratum Conreum of Atopic Dermatits: An Etioogic Factor in Atopic Dry Skin? J. Invest. Dermatol. 96 (1991) 523–526.

[12] S. Motta, M. Monti, S. Sesana, R. Caputo, S. Carelli, R. Ghidoni, Ceramide composition of the psoriatic scale, BBA - Mol. Basis Dis. 1182 (1993) 147–151, https://doi.org/10.1016/0925-4439(93)90135-N.

[13] F.F. Sahle, J. Wohlrab, R.H.H. Neubert, Controlled penetration of ceramides into and across the stratum corneum using various types of microemulsions and formulation associated toxicity studies, Eur. J. Pharm. Biopharm. 86 (2014) 244–250, https://doi.org/10.1016/j.ejpb.2013.07.011.

[14] F.F. Sahle, H. Metz, J. Wohlrab, R.H.H. Neubert, Lecithin-based microemulsions for targeted delivery of Ceramide AP into the stratum corneum: Formulation, characterizations, and in vitro release and penetration studies, Pharm. Res. 30 (2013) 538–551, https://doi.org/10.1007/s11095-012-0899-x.

[15] S. Heuschkel, A. Goebel, R.H.H. Neubert, Microemulsions—Modern Colloidal Carrier for Dermal and Transdermal Drug Delivery, J. Pharm. Sci. 97 (2008) 603–631, https://doi.org/10.1002/jps.20995.

[16] R. Abdelgawad, M. Nasr, N.H. Moftah, M.Y. Hamza, Phospholipid membrane tubulation using ceramide doping “Cerosomes”: Characterization and clinical application in psoriasis treatment, Eur. J. Pharm. Sci. 101 (2017) 258–268, https://doi.org/10.1016/j.ejps.2017.02.030.

[17] A. Vovesná, A. Zhigunov, M. Balouch, J. Zbytovská, Ceramide liposomes for skin barrier recovery: A novel formulation based on natural skin lipids, Int. J. Pharm. 596 (2021), https://doi.org/10.1016/j.ijpharm.2021.120264.

[18] Y. Masukawa, J. Ishikawa, R. Homma, H. Narita, T. Kitahara, A. Naoe, Y. Takagi, H. Sato, T. Oba, N. Kondo, Y. Sugai, Comprehensive quantification of ceramide species in human stratum corneum, J. Lipid Res. 50 (2009) 1708–1719, https://doi.org/10.1194/jlr.d800055-jlr200.

[19] R. Kindt, L. Jorge, E. Dumont, P. Couturon, F. David, P. Sandra, K. Sandra, Profiling and Characterizing Skin Ceramides Using Reversed-Phase Liquid Chromatography – Quadrupole Time-of-Flight Mass Spectrometry, Anal. Chem. 84 (2011) 403–411, https://doi.org/10.1021/ac202646v.

[20] J.N. Israelachvili, Intermolecular and Surface Forces, 3rd ed., 2011. https://doi.org/10.1016/C2009-0-21560-1.

[21] V.V. Kumar, Complementary molecular shapes and additivity of the packing parameter of lipids, Proc. Natl. Acad. Sci. U. S. A. 88 (1991) 444–448, https://doi.org/10.1073/pnas.88.2.444.

[22] E. Khazanov, A. Priev, J.P. Shillemans, Y. Barenholz, Physicochemical and biological characterization of ceramide-containing liposomes: Paving the way to ceramide therapeutic application, Langmuir 24 (2008) 6965–6980, https://doi.org/10.1021/la800207z.

[23] J. Mueller, J.S.L. Oliveira, R. Barker, M. Trapp, A. Schroeter, G. Brezesinski, R.H. H. Neubert, The effect of urea and taurine as hydrophilic penetration enhancers on stratum corneum lipid models, Biochim. Biophys. Acta - Biomembr. 1858 (2016) 2006–2018, https://doi.org/10.1016/j.bbamem.2016.05.010.

[24] A. Fathi-Azarbayjani, K.X. Ng, Y.W. Chan, S.Y. Chan, Lipid Vesicles for the Skin Delivery of Diclofenac: Cerosomes vs. Other Lipid Suspensions, Adv. Pharm. Bull. 5 (2015) 25–33, https://doi.org/10.5681/apb.2015.004.

[25] J.E. Chang, H.J. Cho, E. Yi, D.D. Kim, S. Jheon, Hypocrellin B and paclitaxel-encapsulated hyaluronic acid-ceramide nanoparticles for targeted photodynamic therapy in lung cancer, J. Photochem. Photobiol. B Biol. 158 (2016) 113–121, https://doi.org/10.1016/j.jphotobiol.2016.02.035.

[26] S.M. Jung, G.H. Yoon, H.C. Lee, M.H. Jung, S. Il Yu, S.J. Yeon, S.K. Min, Y.S. Kwon, J.H. Hwang, H.S. Shin, Thermodynamic Insights and Conceptual Design of Skin-Sensitive Chitosan Coated Ceramide/PLGA Nanodrug for Regeneration of Stratum Corneum on Atopic Dermatitis, Sci. Rep. 5 (2015) 1–12, https://doi.org/10.1038/srep18089.

[27] G.Y. Noh, J.Y. Suh, S.N. Park, Ceramide-based nanostructured lipid carriers for transdermal delivery of isoliquiritigenin: Development, physicochemical characterization, and in vitro skin permeation studies, Korean J. Chem. Eng. 34 (2017) 400–406, https://doi.org/10.1007/s11814-016-0267-3.

[28] A.D. Bangham, M.M. Standish, J.C. Watkins, Diffusion of univalent ions across the lamellae of swollen phospholipids, J. Mol. Biol. 13 (1965) 238–252, https://doi.org/10.1016/S0022-2836(65)80093-6.

[29] C.H. Tian, G. Zoriniants, R. Gronheid, M. Van Der Auweraer, F.C. De Schryver, Confocal fluorescence microscopy and AFM of thiacyanine J aggregates in Langmuir-Schaefer monolayers, Langmuir 19 (2003) 9831–9840, https://doi.org/10.1021/la034817s.

[30] K. Kjaer, Some simple ideas on X-ray reflection and grazing-incidence diffraction from thin surfactant films, Phys. B Phys. Condens. Matter. 198 (1994) 100–109, https://doi.org/10.1016/0921-4526(94)90137-6.

[31] F. Strati, R.H.H. Neubert, L. Opálka, A. Kerth, G. Brezesinski, Non-ionic surfactants as innovative skin penetration enhancers: insight in the mechanism of interaction with simple 2D stratum corneum model system, Eur. J. Pharm. Sci. 157 (2020), https://doi.org/10.1016/j.ejps.2020.105620.

[32] T. Schmitt, S. Lange, B. Dobner, S. Sonnenberger, T. Hauß, R.H.H. Neubert, Investigation of a CER[NP]- and [AP]-Based Stratum Corneum Modeling Membrane System: Using Specifically Deuterated CER Together with a Neutron Diffraction Approach, Langmuir 34 (2018) 1742–1749, https://doi.org/10.1021/acs.langmuir.7b01848.

[33] C. Stefaniu, G. Brezesinski, H. Möhwald, Langmuir monolayers as models to study processes at membrane surfaces, Adv. Colloid Interface Sci. 208 (2014) 197–213, https://doi.org/10.1016/j.cis.2014.02.013.

[34] D. Kessner, A. Ruettinger, M.A. Kiselev, S. Wartewig, R.H.H. Neubert, Properties of ceramides and their impact on the stratum corneum structure: A review - Part 2: Stratum corneum lipid model systems, Skin Pharmacol. Physiol. 21 (2008) 58–74, https://doi.org/10.1159/000112956.

[35] J.A. Bouwstra, G.S. Gooris, F.E.R. Dubbelaar, M. Ponec, Phase behavior of lipid mixtures based on human ceramides: Coexistence of crystalline and liquid phases, J. Lipid Res. 42 (2001) 1759–1770, https://doi.org/10.1016/s0022-2275(20)31502-9.

[36] C. Das, P.D. Olmsted, The physics of stratum corneum lipid membranes, Philos. Trans. R. Soc. A Math. Phys. Eng. Sci. 374 (2016), https://doi.org/10.1098/rsta.2015.0126.

[37] I. Iwai, H. Han, L. Den Hollander, S. Svensson, L.G. Öfverstedt, J. Anwar, J. Brewer, M. Bloksgaard, A. Laloeuf, D. Nosek, S. Masich, L.A. Bagatolli, U. Skoglund, L. Norlén, The human Skin barrier is organized as stacked bilayers of fully extended ceramides with cholesterol molecules associated with the ceramide sphingoid moiety, J. Invest. Dermatol. 132 (2012) 2215–2225, https://doi.org/10.1038/jid.2012.43.

[38] C. Stefaniu, G. Brezesinski, X-ray investigation of monolayers formed at the soft air/water interface, Curr. Opin. Colloid Interface Sci. 19 (2014) 216–227, https://doi.org/10.1016/j.cocis.2014.01.004.

[39] G. Brezesinski, E. Schneck, Investigating Ions at Amphiphilic Monolayers with X-ray Fluorescence, Langmuir 35 (2019) 8531–8542, https://doi.org/10.1021/acs.langmuir.9b00191.

[40] M. Rabionet, K. Gorgas, R. Sandhoff, Ceramide synthesis in the epidermis, Biochim. Biophys. Acta - Mol. Cell Biol. Lipids. 1841 (2014) 422–434, https://doi.org/10.1016/j.bbalip.2013.08.011.

[41] J. Van Smeden, M. Janssens, G.S. Gooris, J.A. Bouwstra, The important role of stratum corneum lipids for the cutaneous barrier function, Biochim. Biophys. Acta - Mol. Cell Biol. Lipids. 1841 (2014) 295–313, https://doi.org/10.1016/j.bbalip.2013.11.00.

[42] B.A. Čuříková-Kindlová, O. Diat, F. Štěpánek, K. Vávrová, J. Zbytovská, Probing the interactions among sphingosine and phytosphingosine ceramides with non- and alpha-hydroxylated acyl chains in skin lipid model membranes, Int. J. Pharm. 563 (2019) 384–394, https://doi.org/10.1016/j.ijpharm.2019.04.010.

[43] J. Zbytovská, M.A. Kiselev, S.S. Funari, V.M. Garamus, S. Wartewig, K. Palát, R. Neubert, Colloids and Surfaces A : Physicochemical and Engineering Aspects Influence of cholesterol on the structure of stratum corneum lipid model membrane, 328 (2008) 90-99. https://doi.org/10.1016/j.colsurfa.2008.06.032.

[44] F. Arends, H. Chaudhary, P. Janmey, M.M.A.E. Claessens, O. Lieleg, Lipid Head Group Charge and Fatty Acid Configuration Dictate Liposome Mobility in Neurofilament Networks, 201600229 (n.d.) 2016 1-8. https://doi.org/10.1002/mabi.201600229.

[45] P. Dreher, F. Walde, P. Luisi, P.L. Elsner, Human skin irritation studies of a lecithin microemulsion gel and of lecithin liposomes, Ski. Pharmacol. (1996) 124–126.

[46] B. Heurtault, P. Saulnier, B. Pech, J.E. Proust, J.P. Benoit, Physico-chemical stability of colloidal lipid particles, Biomaterials 24 (2003) 4283–4300, https://doi.org/10.1016/S0142-9612(03)00331-4.

[47] P.J. Kadu, S.S. Kushare, D.D. Thacker, S.G. Gattani, Enhancement of oral bioavailability of atorvastatin calcium by self-emulsifying drug delivery systems (SEDDS), Pharm. Dev. Technol. 16 (2011) 65–74, https://doi.org/10.3109/10837450903499333.

[48] H. Lambers, S. Piessens, A. Bloem, H. Pronk, P. Finkel, Natural skin surface pH is on average below 5, which is beneficial for its resident flora, Int. J. Cosmet. Sci. 28 (2006) 359–370, https://doi.org/10.1111/j.1467-2494.2006.00344.x.

[49] J. Blaak, P. Staib, The Relation of pH and Skin Cleansing, Curr. Probl. Dermatology. 54 (2018) 132–142, https://doi.org/10.1159/000489527.

[50] A. Blume, A. Kerth, Peptide and protein binding to lipid monolayers studied by FT-IRRA spectroscopy, Biochim. Biophys. Acta - Biomembr. 1828 (2013) 2294–2305, https://doi.org/10.1016/j.bbamem.2013.04.014.

[51] G. Brezesinski, H. Möhwald, Langmuir monolayers to study interactions at model membrane surfaces, Adv. Colloid Interface Sci. 100-102 (2003) 563–584, https://doi.org/10.1016/S0001-8686(02)00071-4.

[52] A. Schlaich, A.P. Dos Santos, R.R. Netz, Simulations of Nanoseparated Charged Surfaces Reveal Charge-Induced Water Reorientation and Nonadditivity of Hydration and Mean-Field Electrostatic Repulsion, Langmuir 35 (2019) 551–560, https://doi.org/10.1021/acs.langmuir.8b03474.

[53] L. Fumagalli, A. Esfandiar, R. Fabregas, S. Hu, P. Ares, A. Janardanan, Q. Yang, B. Radha, T. Taniguchi, K. Watanabe, G. Gomila, K.S. Novoselov, A.K. Geim, Anomalously low dielectric constant of confined water, Science (80-.) 360 (2018) 1339–1342, https://doi.org/10.1126/science.aat4191.

[54] T. Mukhina, A. Hemmerle, V. Rondelli, Y. Gerelli, G. Fragneto, J. Daillant, T. Charitat, Attractive Interaction between Fully Charged Lipid Bilayers in a Strongly Confined Geometry, J. Phys. Chem. Lett. 10 (2019) 7195–7199, https://doi.org/10.1021/acs.jpclett.9b02804.
[55] V.M. Latza, B. Demé, E. Schneck, Membrane Adhesion via Glycolipids Occurs for Abundant Saccharide Chemistries, Biophys. J. 118 (2020) 1602–1611, https://doi.org/10.1016/j.bpj.2020.02.003.
[56] T.J. Mcintosh, A.D. Magid, S.A. Simon, Cholesterol Modifies the Short-Range Repulsive Interactions between Phosphatidylcholine Membranes, Biochemistry 28 (1989) 17–25, https://doi.org/10.1021/bi00427a004.
[57] M.E. Rerek, B.Markovic Chen, D. Van Wyck, P. Garidel, R. Mendelsohn, D. J. Moore, Phytosphingosine and Sphingosine Ceramide Headgroup Hydrogen Bonding: Structural Insights through Thermotropic Hydrogen/Deuterium Exchange, J. Phys. Chem. B. 105 (2001) 9355–9362, https://doi.org/10.1021/jp0118367.
[58] S. Raudenkolb, S. Wartewig, R.H.H. Neubert, Polymorphism of ceramide 6 : a vibrational spectroscopic and X-ray powder diffraction investigation of the diastereomers of N-(alpha-hydroxyoctadecanoyl)-phytosphingosine, Chem. Phys. Lipids. 133 (2005) 89–102, https://doi.org/10.1016/j.chemphyslip.2004.09.015.
[59] T.N. Engelbrecht, A. Schroeter, T. Hauß, B. Demé, H.A. Scheidt, D. Huster, R.H. H. Neubert, The impact of ceramides NP and AP on the nanostructure of stratum corneum lipid bilayer. Part I: Neutron diffraction and 2H NMR studies on multilamellar models based on ceramides with symmetric alkyl chain length distribution, Soft Matter 8 (2012) 6599–6607, https://doi.org/10.1039/c2sm25420d.
[60] B. Skolova, B. Janusova, J. Zbytovska, G. Gooris, J.A. Bouwstra, P. Slepička, P. Berka, J. Roh, K. Palát, A. Hrabálek, K. Vavrova, Ceramides in the Skin Lipid Membranes: Length Matters, Langmuir. 29 (2013) 15624–15633.
[61] P. Pullmannová, L. Pavlíková, A. Kováčik, M. Sochorová, B. Školová, P. Slepička, J. Maixner, J. Zbytovská, K. Vávrová, Permeability and microstructure of model stratum corneum lipid membranes containing ceramides with long (C16) and very long (C24) acyl chains, Biophys. Chem. 224 (2017) 20–31, https://doi.org/10.1016/j.bpc.2017.03.004.